



Improvement of photocatalytic activity under visible-light irradiation by heterojunction of Cu ion loaded WO_3 and Cu ion loaded N-TiO₂



Tomoya Iihoshi^a, Takeshi Ohwaki^{a,*}, Junie Jhon M. Vequizo^b, Akira Yamakata^b

^a Graduate School of Science and Technology, Meijo University, 1-501 Shiogamaguchi, Tempaku, Nagoya 468-8502, Japan

^b Graduate School of Engineering, Toyota Technological Institute, Toyota Technological Institute, 2-12-1 Hisakata, Tempaku, Nagoya 468-8511, Japan

ARTICLE INFO

Keywords:

Photocatalyst
Heterojunction
Charge transfer
Composites

ABSTRACT

Visible-light-sensitive photocatalysts have frequently been used for indoor environmental purification. In order to further expand the applications, improvements in photocatalytic performance are desired. In this study, we have prepared new composite photocatalysts with copper ion loaded tungsten trioxide (Cu/WO_3) and copper ion loaded nitrogen-doped titanium dioxide ($\text{Cu}/\text{N-TiO}_2$) as a function of the composition ratio. Acetaldehyde decomposition activities under visible-light irradiation have been significantly enhanced by the heterojunction photocatalysts at a composition ratio of 1:9 against Cu/WO_3 and $\text{Cu}/\text{N-TiO}_2$. We have also investigated the enhanced mechanisms of the photocatalytic activity using time-resolved visible to mid-infrared (mid-IR) absorption spectroscopy. It has been revealed that there are longer hole lifetimes via electron transfer from the conduction bands of N-TiO₂ and WO₃ to Cu ions, and hole transfer from the valence band of WO₃ to that of N-TiO₂.

1. Introduction

Photocatalysts such as TiO₂ have been used for environmental purification [1,2]. In particular, ultraviolet- (UV-) light-sensitive photocatalysts have been used as self-cleaning building materials (e.g., on outer walls, window glass and tents) by utilizing hydrophilic surfaces. However, the photocatalytic functions of TiO₂ only occur under UV irradiation because the TiO₂ bandgap is 3.2 eV for anatase and 3.0 eV for rutile, and TiO₂ light absorption is limited to wavelengths shorter than 380–400 nm. Therefore, in order to utilize photocatalysts in interior illumination condition, previous studies have analyzed visible-light-sensitive photocatalysts and developed them for indoor environmental purification. As a result, various types of visible-light-sensitive photocatalysts have been proposed [3–5], which include (1) metal-doped TiO₂, (2) anion-doped TiO₂, (3) sensitized TiO₂, and (4) metal ion loaded TiO₂ or WO₃. Metal-doped TiO₂ photocatalysts have been developed using either ion implantation methods [6,7] or sol-gel methods [8–10]. Previous research suggests that metal ions such as Cr³⁺ substitute at Ti⁴⁺ sites in the TiO₂ lattice, resulting in visible-light absorption [6]. Anion-doped TiO₂ photocatalysts have been developed using dry and wet processes. For example, Asahi et al. have reported that N-doped TiO₂, prepared by TiO₂ sputter deposition in an Ar and N₂ mixed gas or NH₃ annealing of TiO₂ powders, exhibits enhanced visible-light absorption and photocatalytic activity under conditions of visible-

light irradiation [11,12]. Furthermore, various anion-doped (C [13–15], F [16,17], S [15,18,19]) TiO₂ photocatalysts have been found to be visible responsible. Typical sensitized TiO₂ photocatalysts have been created via modification of metal complex [3,5,20–22], prepared mainly by a solution impregnation process. Metal ion loaded TiO₂ or WO₃ photocatalysts have been mainly developed by combining Cu(II) ions and TiO₂ or WO₃ [23–25], usually prepared by oxide powder impregnation in an aqueous solution. The improvement of visible-light sensitivity has been explained by Cu ion reduction reaction via electron transfer from the oxide valence band.

In order to further improve photocatalytic activity under visible-light irradiation, experiments in previous studies have been performed to co-dope metal ions and anions [26–28] or to combine anion doping and metal ion loading [29–31]. In recent years, new visible-light-sensitive photocatalysts have been investigated. The combination of heterogeneous semiconductors is one of the new photocatalysts. Experiments performed by Etacheri et al. have revealed that nitrogen-doped anatase-rutile heterojunctions have high photocatalytic activity under visible-light irradiation [32]. Wang and coworkers have reviewed type-II heterostructures, focusing particularly on TiO₂ and ZnO based photocatalysts [33]. Moreover, various strategies for efficient visible-light-sensitive photocatalysts have been proposed [4], especially for black TiO₂ [34] and plasmonic Au-TiO₂ [35] photocatalysts.

Among these developed visible-light-sensitive photocatalysts,

* Corresponding author.

E-mail address: ohwaki@meijo-u.ac.jp (T. Ohwaki).

anion-doped TiO_2 or metal ion loaded TiO_2 and WO_3 are currently used for practical interior application such as antibacterial, antiviral, harmful gas decomposition, and deodorants etc [12,36]. To expand the application of environmental purification, further development of more active visible-light-sensitive photocatalyst is required.

On the other hand, in order to improve photocatalytic activity, understanding the photocatalytic reaction mechanisms through the investigation of photo-generated electron and hole behaviors in the photocatalysts is important. In particular, understanding of the charge carrier transfer between the photocatalysts such as TiO_2 or WO_3 and loading ions, and between heterojunctions. Time-resolved absorption spectroscopy from visible to mid-IR wavelength is a powerful method to study the behavior of photo-generated electrons and holes [37–41]. In the visible to near-IR regions, holes and deeply trapped electrons give characteristic absorption peak, so spectroscopy has been applied to investigate the behavior of photo generated holes and deeply trapped electrons. Moreover, relationship between the photocatalytic activities under visible-light irradiation and electron and hole behaviors by UV laser excitation has been clarified in anion-doped TiO_2 [42,43].

In this study, we have attempted to improve photocatalytic activity under visible-light irradiation by heterojunction of Cu ion loaded tungsten oxide (Cu/WO_3) and Cu ion loaded N-doped titanium oxide ($\text{Cu}/\text{N-TiO}_2$), which are put into practical use as material systems. Specifically, we have investigated to improve the photocatalytic activity by optimizing the Cu/WO_3 composition ratio with $\text{Cu}/\text{N-TiO}_2$. We have then analyzed the photocatalytic activities by measuring the decomposition rates of acetaldehyde and generation rates of CO_2 under visible-light irradiation. Moreover, we have investigated the lifetime and behavior of photo generated charge carriers by performing femtosecond time-resolved visible to mid-IR absorption measurements.

2. Experimental

2.1. Photocatalytic powder preparation

The impregnation method was used to prepare Cu/WO_3 . A commercial form of WO_3 (Kanto Chemical Co., Inc., Japan) was chosen as a representative photocatalytic powder. WO_3 powders were suspended in water with $\text{Cu}(\text{NO}_3)_2$ (Wako Pure Chemical Industries, Japan) and stirred for 3 h. The amount of $\text{Cu}(\text{NO}_3)_2$ was adjusted such that the final calculated Cu^{2+} -to- WO_3 powder mass ratio was 0.2%. After stirring, the samples were dried at 353 K and then heat-treated at 773 K in the atmosphere. $\text{Cu}/\text{N-TiO}_2$ powders were sourced from Toyota Tsusho Co., Ltd./Toyotsu Vehitecs Co., Ltd. The characteristics of the $\text{Cu}/\text{N-TiO}_2$ photocatalyst have been presented elsewhere [44].

The prepared Cu/WO_3 powders were mixed with the $\text{Cu}/\text{N-TiO}_2$ powders at a predetermined mixing ratio (Cu/WO_3 ratio = 50, 33, 25, and 10 wt%), stirred in water for 30 min, and then dried. These samples are denoted as “ $\text{Cu}/\text{WO}_3/\text{Cu}/\text{N-TiO}_2(m:n)$ ” (m:n means the ratio of Cu/WO_3 to $\text{Cu}/\text{N-TiO}_2$). For example, “ $\text{Cu}/\text{WO}_3:\text{Cu}/\text{N-TiO}_2(1:9)$ ” indicates that Cu/WO_3 : $\text{Cu}/\text{N-TiO}_2$ = 1:9. The Cu ion loaded ratios were measured by an X-ray Fluorescence (XRF) spectrometer (Rigaku, Supermini 2000, Japan). The specific surface area (SSA) was analyzed from the amount of nitrogen adsorbed at the temperature of liquid nitrogen by using a BET adsorption isotherm (Autosorb-1, Quantachrome Instruments). The structure of mixed samples were observed by a secondary electron micrograph. The absorption spectra for the Cu/WO_3 , $\text{Cu}/\text{N-TiO}_2$, and $\text{Cu}/\text{WO}_3:\text{Cu}/\text{N-TiO}_2(1:9)$ powders were measured for comparison.

2.2. Photocatalytic properties

The photocatalytic activity of each sample was evaluated using the gaseous acetaldehyde photo decomposition rates and CO_2 generation rates under visible-light irradiation for 24 h. Each 0.1 g sample was placed into a 500 cc glass vessel. Dry air and acetaldehyde (initial

concentration of 1000 ppm) gas were then introduced into the vessel. The vessels were placed under dark condition for 24 h, and the acet-aldehyde and CO_2 concentrations were measured under visible-light irradiation with a white LED lamp (1.0 mW/cm² at 450 nm peak wavelength). Gas concentrations were measured using gas chromatograph (Shimadzu, GC-2014, Japan).

2.3. Time-resolved visible to mid-IR absorption measurements

Microsecond to millisecond time-resolved absorption measurements were performed in the visible to mid-IR region (25,000–1000 cm⁻¹) using the pump-probe method based on a Nd:YAG laser system (Continuum, Surelite I; duration: 6 ns, power: 0.5 mJ, repetition rate: 10–0.01 Hz). The details of the time-resolved absorption measurements have been previously reported.^{37, 39} In this experiment, a 355 nm pulse was used to excite the charge carriers in the photocatalyst powder, since we want to measure the transient absorption as wide as possible. $\text{Cu}/\text{N-TiO}_2$ and Cu/WO_3 absorb visible light but visible pump pulse (< 500 nm) disables the measurements below 20,000 cm⁻¹ (500 nm). UV pulse enables the measurements from 25,000 to 1000 cm⁻¹ (400 nm ~ 10 μm), and is useful to observe the charge transfers between $\text{Cu}/\text{N-TiO}_2$ and Cu/WO_3 . The IR light coming from a MoSi₂ coil and the visible to NIR light, originating from a halogen lamp, were utilized to probe the charge carriers in the mid-IR and visible to NIR regions, respectively. In the mid-IR region (6000–1000 cm⁻¹), measurements were performed in transmission mode; that is, probe light transmitted from the sample was detected by an MCT detector (Kolmar). On the other hand, in the visible to NIR region (25,000–6000 cm⁻¹), measurements were carried out in reflection mode; that is, diffuse reflected probe light from the sample was detected by either Si or InGaAs detectors. An AC-coupled amplifier (Stanford Research Systems, SR560, 1 MHz) was used to amplify the electric signal output. The time resolution of the spectrometers was limited to 1–2 μs by the bandwidth of the amplifier. The decay kinetics and the reactivity of photocarriers were determined by measuring the changes in the absorbance intensity of N_2 or under O_2 gas or MeOH vapor (with a pressure of 20 Torr) at room temperature.

3. Results and discussion

3.1. Photocatalytic activities for acetaldehyde decomposition

The photocatalytic activity for the samples was estimated by measuring the acetaldehyde decomposition rates and the CO_2 generation rates. Since the vessels were placed under dark condition for 24 h after acetaldehyde gas introduction, the acetaldehyde concentrations at the start of photo decomposition depended on the samples. The concentrations for the Cu/WO_3 and $\text{Cu}/\text{N-TiO}_2$ were 600 ppm and 10 ppm, respectively. The amount of acetaldehyde gas adsorbed in $\text{Cu}/\text{N-TiO}_2$ powder was very high. This is due to the larger surface area in the $\text{Cu}/\text{N-TiO}_2$ powder, whereas the Cu/WO_3 powder has a smaller surface area. The concentrations for the composites were nearly proportional to the mixing ratio of Cu/WO_3 and $\text{Cu}/\text{N-TiO}_2$. Therefore, the acet-aldehyde decomposition rates and the CO_2 generation rates in the initial stage were affected by the initial adsorption amounts, as described above.

Accordingly, photocatalytic activities were evaluated on the basis of CO_2 evolution after 24 h for various weight mixing ratios, as shown in Fig. 1. It was found from Fig. 1 that the amount of CO_2 increased with increasing the ratio of $\text{Cu}/\text{N-TiO}_2$ and that CO_2 generation was maximized when the compositional ratios of Cu/WO_3 and $\text{Cu}/\text{N-TiO}_2$ were 1: 9. We clearly observed the heterojunction effect in Cu/WO_3 and $\text{Cu}/\text{N-TiO}_2$ during CO_2 evolution.

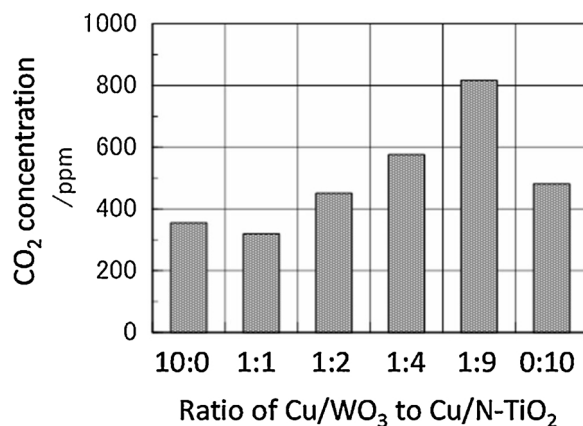


Fig. 1. Photocatalytic activities of the composites photocatalyst powders with Cu/WO₃ and Cu/N-TiO₂. The activities are evaluated by the amounts of CO₂ produced after 24 h under white LED light irradiation.

3.2. Physical properties of Cu/WO₃, Cu/N-TiO₂, and the composites

The crystallite size and SSA of Cu/WO₃, Cu/N-TiO₂ and the composites were evaluated by the X-ray diffraction peak width using the Scherrer equation and the BET adsorption isotherm, respectively. Table 1 lists the values for the crystallite particle size and SSA for Cu/WO₃, Cu/N-TiO₂, and Cu/WO₃:Cu/N-TiO₂(1:9) composite. Cu/WO₃ powder is a coarse particle and has small SSA values. On the other hand, Cu/N-TiO₂ powder is a fine particle and has a large SSA. The SSA values for each mixture correspond to each mixing ratio. The crystallite particle size values are inversely proportional to the SSA values. Moreover, it is confirmed that the SSA values affect the acetaldehyde gas absorption properties as mentioned before.

Fig. 2 shows scanning electron microscope (SEM) images of Cu/WO₃, Cu/N-TiO₂, and Cu/WO₃:Cu/N-TiO₂(1:9) composite. From Fig. 2, we can observe that particle sizes of Cu/WO₃ and Cu/N-TiO₂ are around 50~200 nm and 20~40 nm, respectively. These particle sizes corresponded to the crystallite particle sizes shown in Table 1. The SEM image of (c) Cu/WO₃:Cu/N-TiO₂(1:9) composite was exactly the same as that of (b) Cu/N-TiO₂ at various observation points. Particles of Cu/WO₃ could not be observed at all in the SEM image of (c) Cu/WO₃:Cu/N-TiO₂(1:9) composite. These results suggest that fine particles (Cu/N-TiO₂) cover large particles (Cu/WO₃ powders) in Cu/WO₃:Cu/N-TiO₂(1:9) composite.

Fig. 3 shows the optical absorption spectra of the previous discussed powders. We observed absorptions in the visible-light region from 400 to 500 nm and above 600 nm in all samples and that Cu/WO₃ absorbed more photons compared with Cu/N-TiO₂ in the 400~500 nm region. The absorption spectra for Cu/WO₃ and Cu/N-TiO₂ were consistent with the results published by Irie et al. [23] and Yamanaka et al. [45], respectively. The absorption edge at 470 nm for Cu/WO₃ powders corresponds to WO₃ bandgap absorption. The absorption at 400~520 nm in the Cu/N-TiO₂ powders is a consequence of the transition from N 2p to Ti 3d(CB). Absorption at 700~800 nm was assigned to the Cu(II) d-d transition [23].

Table 1

Crystallite particle size and SSA of Cu/WO₃, Cu/N-TiO₂, and Cu/WO₃:Cu/N-TiO₂(1:9) powders.

Sample	Crystallite particle size (nm) ^a	SSA (m ² /g)
Cu/WO ₃	72.2	4.5
Cu/N-TiO ₂	30	107.2
Cu/WO ₃ :Cu/N-TiO ₂ (1:9)	93.5(Cu/WO ₃) 31.2(Cu/N-TiO ₂)	93.6

^a The crystallite particle size for Cu/WO₃ was evaluated by d(200).

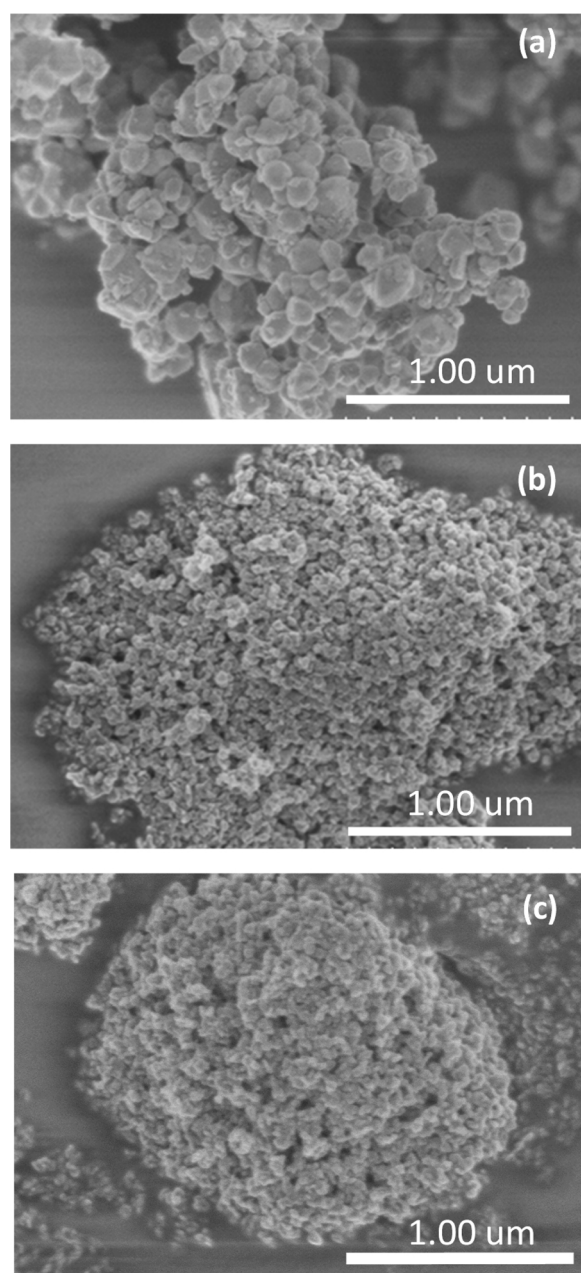


Fig. 2. SEM images of the (a) Cu/WO₃, (b) Cu/N-TiO₂, and (c) Cu/WO₃:Cu/N-TiO₂(1:9) powders.

3.3. Time-resolved absorption measurement

The photogenerated electron/hole behavior was measured by time-resolved absorption measurements. Fig. 4 shows the transient absorption spectra for Cu/WO₃, Cu/N-TiO₂, and Cu/WO₃:Cu/N-TiO₂(1:9) powders induced by 355 nm laser irradiation. Fig. 4 also shows the transient absorption spectra for bare N-TiO₂ powder for comparison. Fig. 4 indicates that broad band absorption was observed over the wave number region of 25,000 to 13,000 cm⁻¹ for N-TiO₂, Cu/N-TiO₂ and Cu/WO₃:Cu/N-TiO₂(1:9), and that a relatively narrow band absorption was observed over the wave number region of 25,000 to 20,000 cm⁻¹ for Cu/WO₃. By comparing Figs. 4(b) and 4(c) with Fig. 4(d), the broad band absorption increased and had longer lifetime by combining Cu/WO₃ and Cu/N-TiO₂. The broad absorption spanning from 25,000 to 13,000 cm⁻¹ is due to the absorption of trapped electrons and/or holes [46]. Fig. 4(a) also indicates that band absorption was observed under

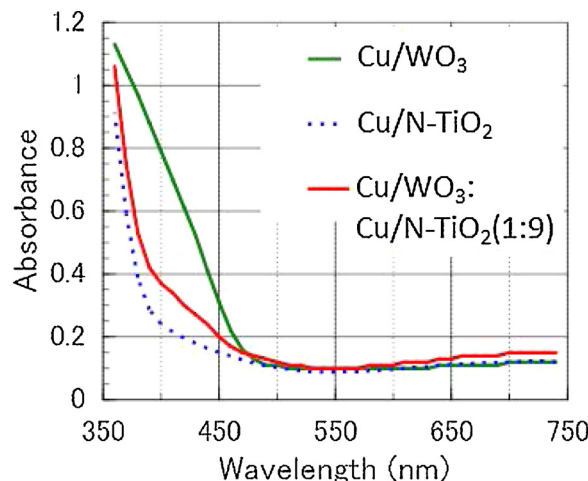


Fig. 3. Absorption spectra for Cu/WO_3 , $\text{Cu}/\text{N-TiO}_2$, and $\text{Cu}/\text{WO}_3:\text{Cu}/\text{N-TiO}_2(1:9)$ powders.

the wave number region of 3000 cm^{-1} for N-TiO_2 . It is known that the band absorption under 3000 cm^{-1} is due to free electrons.^{39, 42, 43} The intensity of free electrons of N-TiO_2 in Fig. 4(a) was more stronger than that of N-TiO_2 shown in the past literature [40,41], which indicates that the number of the defects that trap free electrons is much smaller than other N-TiO_2 catalysts synthesized by the literatures.^{40,41} On the other hand, there were small amounts of band absorption under 3000 cm^{-1} for $\text{Cu}/\text{N-TiO}_2$ and $\text{Cu}/\text{WO}_3:\text{Cu}/\text{N-TiO}_2(1:9)$.

The decay curve measurements in the presence of reactant molecules enable the assignment of the broad absorption at $25,000 \sim 13,000 \text{ cm}^{-1}$. For this experiment, the decay curves at $15,000$ and $20,000 \text{ cm}^{-1}$ for $\text{Cu}/\text{WO}_3:\text{Cu}/\text{N-TiO}_2(1:9)$ were measured (Fig. 5). The results indicate that the absorption intensity changes very little when exposed to oxygen compared with N_2 , whereas the absorption intensity decreases when exposed to CH_3OH . This suggests that broad band

absorption is a consequence of trapped holes. The decay curves for N-TiO_2 , Cu/WO_3 , $\text{Cu}/\text{N-TiO}_2$, and $\text{Cu}/\text{WO}_3:\text{Cu}/\text{N-TiO}_2(1:9)$ powders were compared. Fig. 6 shows the decay curves at 2000 and $17,000 \text{ cm}^{-1}$ for the four powders measured in a vacuum. In order to prevent the signal overlapping with the trapped holes in WO_3 , the decay curves of trapped holes in N-TiO_2 were measured at $17,000 \text{ cm}^{-1}$. From the decay curves for N-TiO_2 and $\text{Cu}/\text{N-TiO}_2$ at 2000 cm^{-1} in Fig. 6, we observe that the existence of Cu ion loaded on N-TiO_2 accelerates the free electron decay, which means rapid electron transfer from N-TiO_2 conduction band to the loaded Cu ions. These results agree with those of Yamanaka et al. [45]. We also observe that the free electron decay in the decay curves for Cu/WO_3 is accelerated by composite with $\text{Cu}/\text{N-TiO}_2$. The decay curve for $\text{Cu}/\text{WO}_3:\text{Cu}/\text{N-TiO}_2(1:9)$ at 2000 cm^{-1} is almost identical to that of $\text{Cu}/\text{N-TiO}_2$, which indicate that electrons migrate to copper ions even during Cu/WO_3 and $\text{Cu}/\text{N-TiO}_2$ composite. Furthermore, as seen Fig. 6, the number of surviving trapped holes increased throughout the time resolution (approximately $2 \mu\text{s}$) for $\text{Cu}/\text{WO}_3:\text{Cu}/\text{N-TiO}_2(1:9)$ composite compared with Cu/WO_3 or $\text{Cu}/\text{N-TiO}_2$, and the decay curves were nearly parallel across the microsecond region. These results suggest that hole transfer from valence band of WO_3 to that of N-TiO_2 within the spectrometer time resolution ($\sim 2 \mu\text{s}$). Heterojunction of Cu/WO_3 and $\text{Cu}/\text{N-TiO}_2$ is thought to have the effect of increasing the number of trapped holes and prolonging the lifetime.

The photocatalytic activity exhibited the most significant improvements when Cu/WO_3 and $\text{Cu}/\text{N-TiO}_2$ were mixed at a ratio of 1: 9, as shown in Fig. 1. The composite powder is composed of relatively coarse Cu/WO_3 powder and fine $\text{Cu}/\text{N-TiO}_2$ powder, where the copper state is $\text{Cu}(\text{OH})_2$ [44]. As shown in Fig. 2, the Cu/WO_3 powder is surrounded by the $\text{Cu}/\text{N-TiO}_2$ powder. Absorbance of Cu/WO_3 near 450 nm is greater than that of $\text{Cu}/\text{N-TiO}_2$, which is shown in Fig. 3. This indicates that 450 nm light is efficiently absorbed by $\text{Cu}/\text{N-TiO}_2$ along exterior and by Cu/WO_3 in the interior. On the other hand, time-resolved absorption spectra of the photocatalytic powders reveal that the lifetime of the holes, generated by photoexcitation, is extended by the heterojunction of Cu/WO_3 and $\text{Cu}/\text{N-TiO}_2$, which is shown in Figs. 4 and 6. This suggests that the holes are likely to move from valence band of

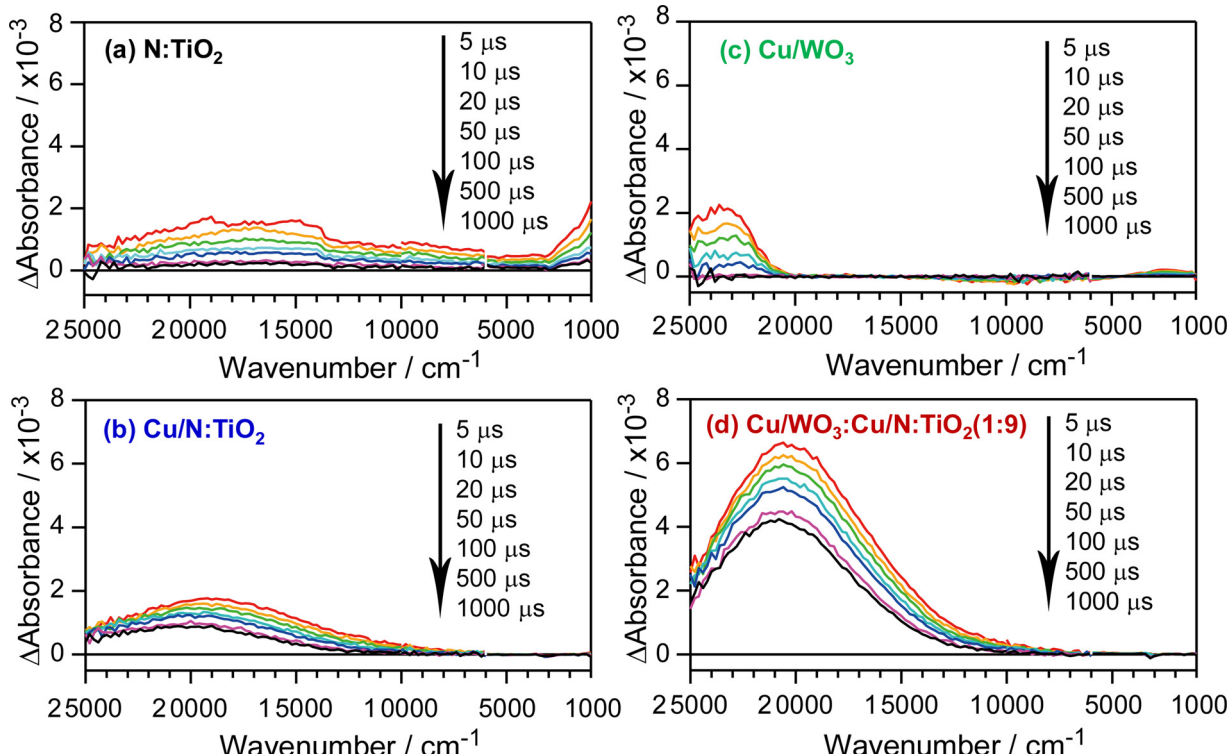


Fig. 4. Time-resolved absorption spectra for the (a) N-TiO_2 , (b) $\text{Cu}/\text{N-TiO}_2$, (c) Cu/WO_3 , and (d) $\text{Cu}/\text{WO}_3:\text{Cu}/\text{N-TiO}_2(1:9)$ photocatalysts.

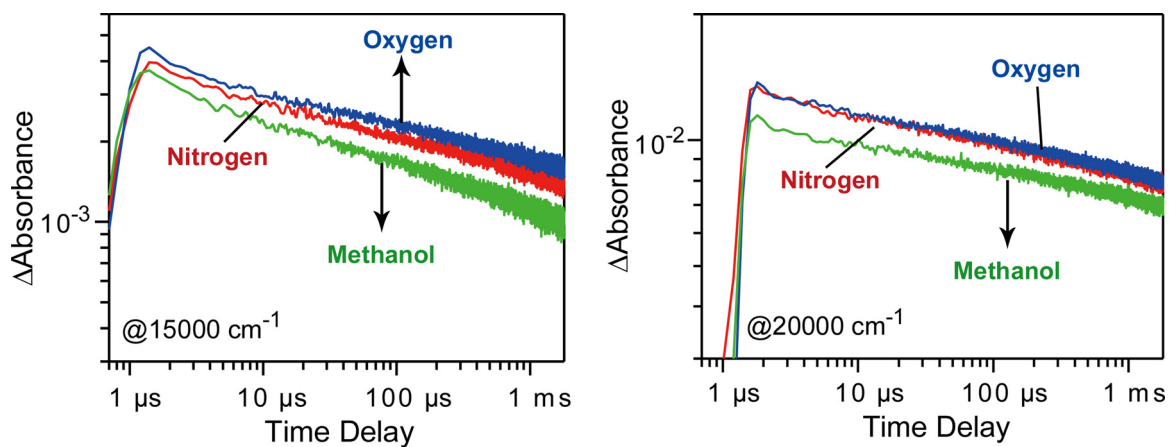


Fig. 5. Transient absorption decay curves for the $\text{Cu}/\text{WO}_3:\text{Cu}/\text{N-TiO}_2(1:9)$ photocatalyst powders probed at $15,000$ and $20,000\text{ cm}^{-1}$ in nitrogen, oxygen, and methanol.

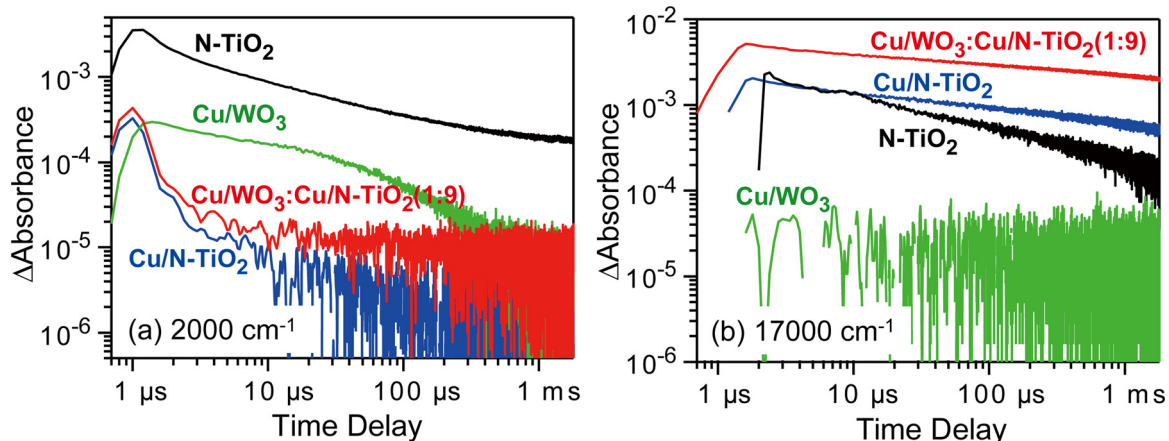


Fig. 6. Transient absorption decay curves for the N-TiO_2 , Cu/WO_3 , $\text{Cu}/\text{N-TiO}_2$, and $\text{Cu}/\text{WO}_3:\text{Cu}/\text{N-TiO}_2(1:9)$ photocatalyst powders measured in a vacuum. The decay curves were probed at 2000 and $17,000\text{ cm}^{-1}$.

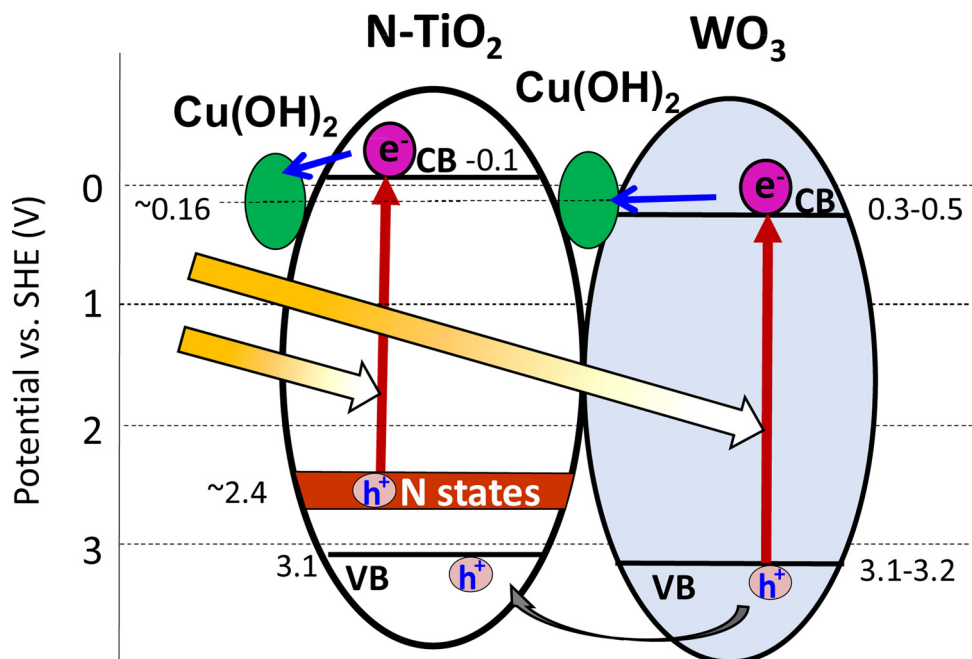


Fig. 7. Schematic illustration of energy diagrams for heterojunction of Cu/WO_3 and $\text{Cu}/\text{N-TiO}_2$.

WO_3 to that of N-TiO₂ on the bases of the relationship between the energy level of the WO_3 and N-TiO₂ valence band. Since N-TiO₂ powders exist outside of the composite, gas oxidation reactions are more likely to occur on the N-TiO₂ surface. Fig. 7] illustrates the schematic energy diagrams of the heterojunction of photocatalytic powders, in which the energy levels referred to the previous works [12,23,47].

To recap, the mechanism of photo-activity improvement is suggested as follows. Visible-light is efficiently absorbed in two stages by the outer N-TiO₂ and the inner WO_3 , concurrently generating electrons and holes in each photocatalyst powder. In N-TiO₂, electron is excited from N 2p state to Ti 3d state [11,12]. In WO_3 , electron is excited from O 2p state to W 5d state [23,47]. The excited electrons are then immediately transferred to the copper ions, and holes generated in the WO_3 are transferred to the N-TiO₂ valence band. Accordingly, it is thought that there exist two states of hole trapping in N-TiO₂, that is N 2p state and O 2p state. This is probably the reason why the heterojunction additionally contribute to the increase of the life time. The holes contribute to the oxidative decomposition of the acetaldehyde gas, whereas electrons transferred to the copper ions promote oxidation reaction via Fenton's reaction [44].

We infer that white LEDs will become popular in future indoor lighting sources. White LEDs are a combination of blue LEDs (peak wavelength of approximately 450 nm) and orange phosphors. The purification of the indoor environments requires a highly active photocatalyst under 450 nm light irradiation.

4. Conclusions

In this study, we investigated the enhancement of photocatalytic activity via the heterojunction of Cu/ WO_3 and Cu/N-TiO₂. The activities for acetaldehyde decomposition under visible-light irradiation were significantly enhanced by heterojunction at a composition ratio of 1: 9 between Cu/ WO_3 and Cu/N-TiO₂. The enhanced photocatalytic activity mechanisms were investigated using time-resolved visible to mid-IR absorption spectroscopy. The results indicates that there are longer hole lifetimes via electron transfer from the conduction bands of N-TiO₂ and WO_3 to Cu ions, and hole transfer from the valence band of WO_3 to that of N-TiO₂.

Acknowledgments

This work was partially supported by JSPS KAKENHI Grant Number 15K05601. We thank to TOYOTA Tsusho Corporation and TOYOTSU Vehitecs Co., Ltd., who provided a part of the samples.

Appendix A. Supplementary data

Supplementary material related to this article can be found, in the online version, at doi:<https://doi.org/10.1016/j.apcatb.2019.01.046>.

References

- [1] K. Hashimoto, H. Irie, A. Fujishima, *Jpn. J. Appl. Phys.* 44 (2005) 8269–8285.
- [2] A. Fujishima, T.N. Rao, D.A. Tryk, *J. Photochem. Photobiol. C* 1 (2000) 1–21.
- [3] X. Chen, S.S. Mao, *Chem. Rev.* 107 (2007) 2891.
- [4] S. Banerjee, S. Pillai, P. Falaras, K.E. O'Shea, J.A. Byrne, D.D. Dionysiou, *J. Phys. Chem. Lett.* 5 (2014) 2543–2554.
- [5] S.G. Kumar, L.G. Devi, *J. Phys. Chem. A* 115 (2011) 13211–13241.
- [6] M. Anpo, *Bull. Chem. Soc. Jpn.* 77 (2004) 1427–1442.
- [7] J. Schneider, M. Matsuoka, M. Takeuchi, J. Zhang, Y. Horiuchi, M. Anpo, D.W. Bahnemann, *Chem. Rev.* 114 (2014) 9919–9986.
- [8] N. Serpone, D. Lawless, J. Disdier, J.-M. Herrmann, *Langmuir* 10 (1994) 643–652.
- [9] N. Nishiyama, K. Kozasa, S. Yamazaki, *Appl. Catal. A* 527 (2016) 109–115.
- [10] S.N.R. Inturi, T. Boningari, M. Suidan, P.G. Smirniotis, *Appl. Catal. B* 144 (2014) 333–342.
- [11] R. Asahi, T. Morikawa, T. Ohwaki, K. Aoki, Y. Taga, *Science* 293 (2001) 269–272.
- [12] R. Asahi, T. Morikawa, H. Irie, T. Ohwaki, *Chem. Rev.* 114 (2014) 9824–9852.
- [13] H. Irie, Y. Watanabe, K. Hashimoto, *Chem. Lett.* 32 (2003) 772–773.
- [14] S. Sakhivel, H. Kisch, *Angew. Chem., Int. Ed.* 42 (2003) 4908–4911.
- [15] T. Tachikawa, S. Tojo, K. Kawai, M. Endo, M. Fujitsuka, T. Ohno, K. Nishijima, Z. Miyamoto, T. Majima, *J. Phys. Chem. B* 108 (2004) 19299–19306.
- [16] A.M. Czoska, S. Livraghi, M. Chiesa, E. Giammolo, S. Agnoil, G. Granozzi, E. Finazzi, C. Di Valentini, G. Pacchioni, *J. Phys. Chem. C* 112 (2008) 8951–8956.
- [17] D. Li, H. Haneda, S. Hishita, N. Ohashi, N.K. Labhsetwar, *J. Fluorine Chem.* 126 (2005) 69.
- [18] T. Umebayashi, T. Yamaki, H. Itoh, K. Asai, *Appl. Phys. Lett.* 81 (2002) 454.
- [19] T. Ohno, M. Akiyoshi, T. Umebayashi, K. Asai, T. Mitsui, M. Matsumura, *Appl. Catal. A* 265 (2004) 115–121.
- [20] H. Kisch, L. Zang, C. Lange, W.F. Maier, C. Antonius, D. Meissner, *Angew. Chem., Int. Ed.* 37 (1998) 3034–3036.
- [21] W. Macyk, H. Kisch, *Chem. Eur. J.* 9 (2001) 1862–1867.
- [22] Y. Cho, C.H. Choi, C.H. Lee, T. Hyeon, H.I. Lee, *Environ. Sci. Technol.* 35 (2001) 966–970.
- [23] H. Irie, S. Miura, K. Kamiya, K. Hashimoto, *Chem. Phys. Lett.* 457 (2008) 202–205.
- [24] T. Arai, M. Horiguchi, M. Yanagida, T. Gunji, H. Sugihara, K. Sayama, *J. Phys. Chem. C* 113 (2009) 6602–6609.
- [25] X. Qiu, M. Miyauchi, K. Sunada, M. Minoshima, M. Liu, Y. Lu, D. Li, Y. Shimodaira, Y. Hosogi, Y. Kuroda, K. Hashimoto, *Am. Chem. Soc. Nano* 6 (2012) 1609–1618.
- [26] J.H. Xu, J. Li, W.L. Dai, Y. Cao, H. Li, K. Fan, *Appl. Catal. B* 79 (2008) 72–80.
- [27] J.W.J. Hamilton, J.A. Byrne, P.S.M. Dunlop, D.D. Dionysiou, M. Pelaez, K. O'Shea, D. Synnott, S.C. Pillai, *J. Phys. Chem. C* 118 (2014) 12206–12215.
- [28] V. Etacheri, M.K. Seery, S.J. Hinder, S.C. Pillai, *Inorg. Chem.* 51 (2012) 7164–7173 2012.
- [29] T. Morikawa, Y. Irokawa, T. Ohwaki, *Appl. Catal. A* 314 (2006) 123–127.
- [30] T. Morikawa, T. Ohwaki, K.I. Suzuki, S. Moribe, S. Tero-Kubota, *Appl. Catal. B* 83 (2008) 56–62.
- [31] S. Higashimoto, W. Tanihata, Y. Nakagawa, M. Azuma, H. Ohue, Y. Sakata, *Appl. Catal. A* 340 (2008) 98–104.
- [32] V. Etacheri, M.K. Seery, S.J. Hinder, S.C. Pillai, *Chem. Mater.* 22 (2010) 3843–3853.
- [33] Y. Wang, Q. Wang, X. Zhan, F. Wang, M. Safdar, J. He, *Nanoscale* 5 (2013) 8326–8339.
- [34] X. Chen, L. Liu, P.Y. Yu, S.S. Mao, *Science* 331 (2011) 746–750.
- [35] A. Furube, L. Du, K. Hara, R. Katoh, M. Tachiya, *J. Am. Chem. Soc.* 129 (2007) 14852–14853.
- [36] Patent No. EP2248586 A4, US8173573.
- [37] A. Yamakata, M. Kawaguchi, N. Nishimura, T. Minegishi, J. Kubota, K. Domen, *J. Phys. Chem. C* 118 (2014) 23897–23906.
- [38] A. Yamakata, J.J.M. Vequizo, M. Kawaguchi, *J. Phys. Chem. C* 119 (2015) 1880–1885.
- [39] A. Yamakata, J.J.M. Vequizo, H. Matsunaga, *J. Phys. Chem. C* 119 (2015) 24538–24545.
- [40] A. Yamakata, M. Kawaguchi, R. Murachi, M. Okawa, I. Kamiya, *J. Phys. Chem. C* 120 (2016) 7997–8004.
- [41] J.J.M. Vequizo, H. Matsunaga, T. Ishiku, S. Kamimura, T. Ohno, A. Yamakata, *Am. Chem. Soc. Catal.* 7 (2017) 2644–2651.
- [42] S. Komatsuda, Y. Asakura, J.J.M. Vequizo, A. Yamakata, S. Yin, *Appl. Catal. B Environ.* 238 (2018) 358–364.
- [43] A. Nakada, S. Nishioka, J.J.M. Vequizo, K. Muraoka, T. Kanazawa, A. Yamakata, S. Nozawa, H. Kumagai, S. Adachi, O. Ishitani, K. Maeda, *J. Mater. Chem. A* 5 (2017) 11710–11719.
- [44] T. Ohwaki, S. Saeki, K. Aoki, T. Morikawa, *Jpn. J. Appl. Phys.* 55 (2016) 01AA05.
- [45] K. Yamanaka, T. Ohwaki, T. Morikawa, *J. Phys. Chem. C* 117 (2013) 16448–16456.
- [46] A. Yamakata, T. Ishibashi, H. Onishi, *Chem. Phys. Lett.* 333 (2001) 271–277.
- [47] H. Irie, K. Kamiya, T. Shibanuma, S. Miura, D.A. Tryk, T. Yokoyama, K. Hashimoto, *J. Phys. Chem. C* 113 (2009) 10761–10766.